Numerical simulation of electrokinetic dissipation caused by elastic waves in reservoir rocks

Xiaoqian Zhang, Qifei Wang*, Chengwu Li**, Xiaoqi Sun, Zheng Yan and Yao Nie

College of Emergency Management & Safety Engineering, China University of Mining & Technology, Beijing, 100083, China

Abstract. The use of electrokinetic dissipation method to study the fluid flow law in micro-pores is of great significance to reservoir rock microfluidics. In this paper, the micro-capillary theory was combined with the coupling model of the seepage field and the current field under the excitation of the harmonic signal, and the coupling theory of the electrokinetic effect under the first-order approximation condition was derived. The dissipation equation of electrokinetic dissipation and viscous resistance dissipation and its solution were established by using Green's function method. The physical and mathematical models for the electrokinetic dissipation of reservoir rocks were constructed. The microscopic mechanism of the electrokinetic dissipation of reservoir rock were theoretically clarified. The influencing factors of the electrokinetic dissipation frequency of the reservoir rock were analyzed quantitatively. The results show that the electrokinetic effect transforms the fluid flow profile in the pores of the reservoir from parabolic to wavy; under low-frequency conditions, the apparent viscosity coefficient is greater that one and is basically unchanged. The apparent viscosity coefficient gradually approaches 1 as the frequency increases further. The viscous resistance dissipation is two orders of magnitude higher than the electrokinetic effect dissipation. When the concentration of the electrolyte exceeds 0.1mol/L, the electrokinetic dissipation can be neglected, while for the electrolyte solution ($<10^{-2}$M) in low concentration, the electrokinetic dissipation is very significant and cannot be ignored.

Keywords: electrokinetic dissipation; viscous resistance dissipation; viscosity coefficient

1. Introduction

When the elastic wave passes through the formation, it can cause the fluid containing electrolyte to move relative to the rock skeleton, so that the existence of the electric field is observed (Zhang *et al.*2015), and the potential associated with the electric field is called flow potential. The electric field generated by this electrokinetic effect can push excess ions to move in the opposite direction of the pressure gradient, thereby increasing the viscosity of the fluid, consuming energy, slowing the relative motion of the fluid, and thus reducing the attenuation of the wave (Revil *et al.* 2013, Ji and Li 2018). Geophysicists use the electrokinetic coupling phenomenon caused by this elastic wave to identify oil and gas reservoirs in reservoir rocks, monitor the flow of injected water, and evaluate the crack production dynamic monitoring of artificial pressure. As shown in Fig. 1, the pre-designed wavy current is input during the measurement, and the current is input into the formation through the surface electrode (Thompson *et al.* 2007). The electrokinetic effect caused by elastic waves can not only reflect the true flow of fluid in the reservoir, but also its frequency characteristics are similar to those of the excited seismic wave field. Therefore, physicists also use it

to predict the formation properties and observe the earthquake (Liu *et al.* 2018, Jouniaux and Zyserman 2016), etc. The fluid flow in the pores of the reservoir rock belongs to the microfluidic flow, which is different from the phenomenon of macroscopic flow. The existing understanding of microfluidic flow is still in a immature stage. Therefore, it is of great practical and scientific value to deeply study the electrokinetic effect caused by elastic waves in micropores.

There are now two main theological models of electrokinetic coupled waves in reservoir rocks, the Pride model based on the Frenkel theory and the Revil model developed in recent years. According to the basic principles that solid particles and pore solution are guided by respectively, Pride (1994) derived the relation between the frequency and the coupling characteristics of elastic waves and electromagnetic waves in porous media using the method of average volume based on the hypothesis of thin electrical double layer. Revil (2014, 2016) used the basic principles of mechanics and electromagnetics to study the electrokinetic effect of porous media for such rocks with low-porosity and low-permeability as shale by applying the hypothesis of thick electrical double layer, which means the size of its thickness is larger than the porous size. Recently, a kind of electrokinetic coupling model suitable for any pore size was deduced by Shi *et al.* (2018) to study the effect of the thickness of double layer on the electrokinetic effect. As the first one to simulate the electrokinetic coupling effect at borehole in the world, Hu *et al.* (2000) solved the complete equations of Pride model in the axisymmetric cylindrical coordinate system, and deduced

---

*Corresponding author, Ph.D.
  E-mail: wangqf1230@163.com
**Corresponding author, Professor
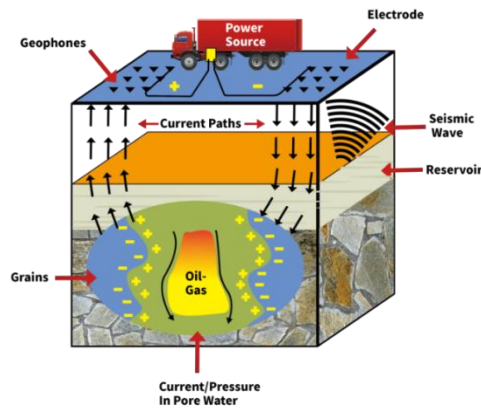 E-mail: lcw@cumtb.edu.cn

Fig. 1 Scheme of field test of electroseismic hydrocarbon detection

the analytical expressions of elastic waves in porous media excited by a monopole point sound source at borehole axis. And thus the full waveform in the time domain of the borehole electrokinetic wave was obtained. Then the rationality and the applicable conditions of calculating borehole seismic wave field by quasi-static field method was justified and presented respectively by Wei *et al.* (2018). And a study about the Joule heat generated by the combined action of pressure drive and electrokinetic drive in a nanochannel was conducted by Zhao *et al.* (2016), which turned out that the heat generated by electrokinetic effect in nanofluids is of great influence on the change of temperature. Ding *et al.* (2019) used circuit analysis to study electrokinetics and thermodynamics, as well as the electrokinetic effects between immiscible liquids, and thus proposed an energy conversion system for nanofluids based on their potential flow. The electrokinetic effect in permafrost was studied by Zyserman *et al.* (2012), who presented numerical examples of detecting natural gas hydrate in permafrost through the conversion of electromagnetic energy and seismic energy by calculating. Besides, Carcione and Tinivella (2000) extended the elastic model of porous media, and presented the mathematical expression of elastic wave propagation in gas hydrate reservoir. Zyserman (2015) studied such shallow questions as the seepage of fluid and the sequestration of carbon dioxide using acoustic logging. In short, the establishment of existing mainstream mathematical models relies on the role of electric double layer. The problem of dynamic electricity effect of reservoir rocks is in the transitional stage from qualitative to quantitative research, and this microfluidic flow also faces many new problems that are different from traditional macroscale flow.

The physical simulation experiment is a research method that can truly reflect the law of the characteristics of the electrokinetic dissipation. Paul Glover (2011) designed a set of measurement methods for studying flow potential in reservoir rock under DC and AC conditions. Imperial College London (Vinogradov and Jackson 2011) designed an experimental device for measuring the coupling coefficient of flow potential in cores, which can eliminate the flow polarization phenomenon. The University of Strasbourg (Allègre *et al.* 2010) designed an experimental device to measure potential, pressure, temperature and cumulative flow rate during fluid flow. Harbin Institute of Technology China (Wang *et al.* 2017) measured and studied the electrokinetic effect in fluid-saturated porous media in laboratory. The electrokinetic conversion signals and interface electrokinetic conversion signals produced by acoustic waves in different model wells were recorded. Holzhauer (2017) experimented with loose sandstone in the frequency range of kilohertz, and investigated the effect of fluid conductivity on the accompanying electric field. The basic information of fluid distribution in the channel was obtained by measuring the value of the adjoint electric field. Garambois (2002) conducted on-site experimental measurements and studies on the electrokinetic effect. Garambois (2002) measured and studied the electrokinetic effect in situ. Two kinds of electromagnetic signals were obtained from the experimental records, i.e. the electromagnetic field induced by sound wave and the adjoining electromagnetic field excited by the discontinuous medium interface. Xie *et al.* (2011) injected bubbles into the pore, which could weaken the electrokinetic effect and increase the flow rate of the fluid. Ghommen *et al.* (2017) carried out an experimental study on the electrokinetic effect under pressure driving. The electrokinetic coupling coefficient obtained from the experiment was compared with the pressure, and a linear relationship was obtained. A field experiment was conducted by Thompson (2007) on natural gas sandstone at depths of 1,000 meters and carbonate reservoirs at depths of 1,500 meters, and he also detected the seismoelectric conversion signal and calculated the magnitude conversion between electromagnetic energy and seismic energy. Last but not least, physical simulation experiments were carried out by Peng et al (2017) on conversion signals of electrokinetic waves at the interface of sandstone samples with wedge shaped models and hole models.

Data analysis shows that the numerical simulation of electrokinetic dissipation can reveal the generation process of electrokinetic dissipation caused by elastic wave from the micro-mechanism, but most work studies electrokinetic effect under stable conditions, or infers electrokinetic dissipation by analyzing velocity field and flow field. However, these methods do not have a unified mathematical analytic formula after all, and can't establish the relationship between parameters and permeability parameters of reservoir rock and macro-electrochemical parameters. This paper aims to answer two questions: (1) What is the micro-mechanism of electrokinetic dissipation in frequency domain of reservoir rock? (2) How to construct mathematical simulation and quantitative calculation methods for describing electrokinetic dissipation? Based on the above problems, the capillary model is used to establish the coupling mathematical model between periodic pressure field and current field. The electro-viscous effect of fluid in reservoir rocks is studied by using the model. The analytical formulas of the electrokinetic effect dissipation function and the viscous resistance dissipation function are derived. The ratio of the two functions is used to quantitatively describe the effect of electrokinetic effect caused by elastic wave on fluid flow. Mathematical method is used to simulate the influence of electrokinetic effect of different reservoir parameters
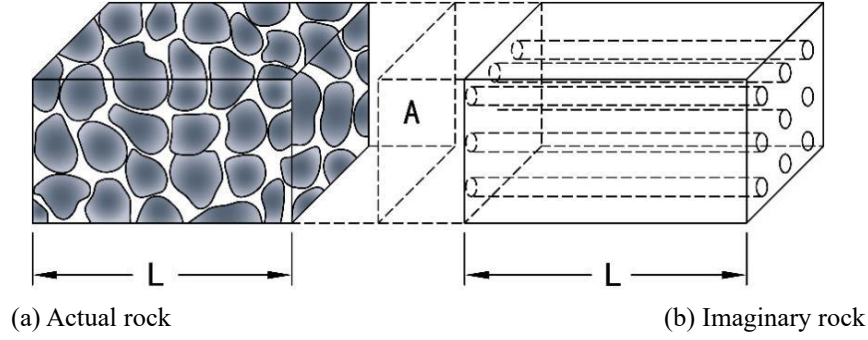
(a) Actual rock   (b) Imaginary rock

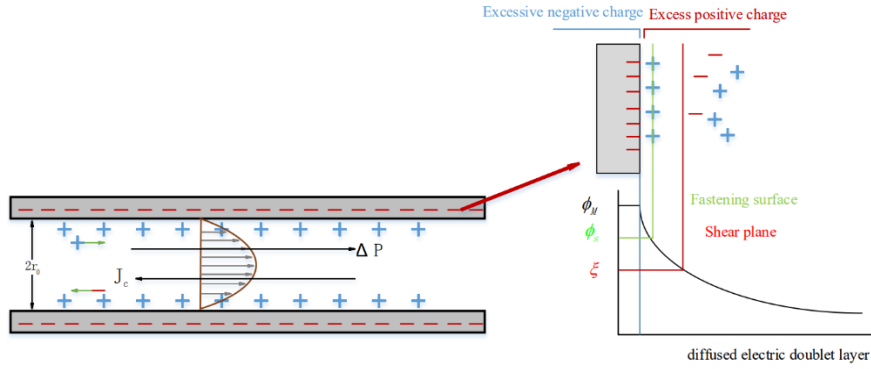Fig. 2 Diameter capillary model

Fig. 3 Sketch of streaming potential

(formation water salinity, cation exchange capacity and porosity) on elastic wave propagation.

2. Electrokinetic coupling model of reservoir rock

2.1 Electric double layer theory of reservoir rock and capillary model

Due to the complexity of pores of actual reservoir rock, it is difficult to establish corresponding mathematical-physical models for related problems. For this reason, simplified models are often used to simulate actual rocks in the study of rock properties. Among them, the circular straight capillary model is the simplest one. In the circular straight capillary model, the pore volume of actual rock can be equivalent to that of capillary with radius. That is to say, a parallel straight capillary is used to replace the pore structure of actual rock, as shown in Fig. 2.

According to the definition of porosity and permeability of reservoir rock, it is easy to get the relationship between micro-parameters of circular straight capillary model and macro-parameters of reservoir rock as

$$\varphi = n_0 \pi r_0^2 \qquad (1)$$

$$k = \frac{n_0 \pi r_0^4}{8} \qquad (2)$$

In the formula, φ is porosity, k is permeability, n_0 is the number of capillaries per unit area and r_0 is the radius of capillaries.

The interaction between reservoir rock skeleton and ion

in solution forms a electric double layer at the interface. In the long straight capillary with radius r_0, the existence of electric double layer makes the ion concentration of multi-electrolyte solution in reservoir obey Boltzmann distribution

$$C_i = C_0 \exp\left(\frac{-Z_i F \psi}{RT}\right) \qquad (3)$$

In the formula: C_i is the concentration of the component i, C_0 is the initial concentration of the solution, $F=9.65\times10^4$C/mol is the Faraday constant, Z_i is the valence of the component i, ψ is the potential formed by the electric double layer, $R=8.314$J(k·mol) is the universal constant of the gas and T is the absolute temperature.

In aqueous solutions with equal positive and negative valence, the charge density in capillaries is derived from the charge conduction theory.

$$\rho_e = FZ(C_+ - C_-) = -2FZC_0 \sinh\left(\frac{ZF\psi}{RT}\right) \qquad (4)$$

According to literature 22, the potential distribution of diffused electric double layer in capillary is as follows

$$\psi = \zeta \exp\left(-\frac{r_0 - r}{\lambda_D}\right) \qquad (5)$$

In the formula, $r_0 = \sqrt{\frac{8k}{\varphi}}$ is the capillary radius;

$\lambda_D = \sqrt{\frac{\varepsilon RT}{2F^2 Z^2 c_0}}$ is the thickness of the double electric layer.

The electric potential ζ on the shear plane of the double layer can be calculated by the cation exchange capacity

Q_V in argillaceous sandstone.

2.2 Electrokinetic effect theory in reservoir rocks

When different pressures P_1 and P_2 are applied to both ends of the formation rock sample, a pressure difference ΔP is generated at both ends of the formation sample, and fluid flow occurs in the formation rock sample. The measuring electrode is placed at both ends of the rock sample, and it will be found that both ends of the rock sample have a potential ΔU. This phenomenon is called the electrokinetic effect, as shown in Fig. 3.

The incompressible fluid in microchannel satisfies the generalized Navier-Stokes equation

$$\psi = \zeta \exp\left(-\frac{r_0 - r}{\lambda_D}\right) \tag{6}$$

In the formula, ρ_0 is the the formation water density in the pores, P is the fluid pressure, u is the flow rate, and μ is the formation water viscosity. Let the electric field strength be the $\mathbf{E} = -\nabla U$, and U is the flow potential.

It is assumed that the pressure gradient caused by the elastic wave in the Z-direction in the rock pore is $\frac{\partial P(z,t)}{\partial z}$, and the pressure field is a harmonic field, that is, $P = P_0 e^{-i\omega t}$. In the formula, $\omega = 2\pi f$, f is the harmonic frequency, and the unit is Hz. The streaming potential stimulated is also a harmonic field, i.e. $U = U_0 e^{-i\omega t}$. Under incompressible conditions, the non-in-phase vibration of pore-solid-liquid interface caused by elastic waves is neglected. The formula (6) is as follows

$$\nabla^2 u + K^2 u = \frac{1}{\mu}(\nabla P + \rho_e \nabla U) \tag{7}$$

In the formula, $K^2 = \frac{i\omega\rho_0}{\mu}$. The formula (7) is the governing equation for fluid flow under the time-harmonic pressure field in the rock pore unit.

The potential boundary conditions and velocity boundary conditions are used: ① at $r=0$, u is a finite value; ② at $r=r_0$, $u=0$, the solution of Eq. (7) is

$$u(r) = \frac{1}{K^2\mu}\left[1 - \frac{J_0(Kr)}{J_0(Kr_0)}\right]\frac{\partial P}{\partial z} - \frac{\varepsilon\zeta}{\mu(1+K^2\lambda_D^2)}\left[\exp\left(-\frac{r_0-r}{\lambda_D}\right) - \frac{J_0(Kr)}{J_0(Kr_0)}\right]\frac{\partial U}{\partial z} \tag{8}$$

In the formula: $J_0(Kr)$ is Bessel zero order function of the first kind.

The formula (8) is the velocity distribution of fluid in pore units.

By integrating the velocity distribution along the capillary section, the flow rate in a single capillary can be obtained

$$Q = \frac{1}{K^2\mu}\left[\pi r_0^2 - \frac{2\pi r_0}{K}\frac{J_1(Kr_0)}{J_0(Kr_0)}\right]\frac{\partial P}{\partial z} + \frac{\varepsilon\zeta}{\mu(1+K^2\lambda_D^2)}\left[\begin{array}{c}\frac{2\pi r_0}{K}\frac{J_1(Kr_0)}{J_0(Kr_0)} \\ -2\pi\left(\lambda_D r_0 - \lambda_D^2 + \lambda_D^2 e^{\frac{-r_0}{\lambda_D}}\right)\end{array}\right]\frac{\partial U}{\partial z} \tag{9}$$

According to the parallel capillary bundle model, pore unit radius $r_0 = \sqrt{\frac{8k}{\varphi}}$, reservoir rock porosity $\varphi = n_0\pi r_0^2$, seepage velocity of reservoir rock $v = n_0 Q$. It can be obtained,

$$v = -\frac{\kappa_D(\omega)}{\mu}\frac{\partial P}{\partial z} - L_{12}\frac{\partial U}{\partial z} \tag{10}$$

The formula (10) is Darcy's Law of seepage velocity in reservoir rocks in frequency domain, $L_{12}\frac{\partial U}{\partial z}$ indicates the seepage excited by flow potential generated by pressure field, which belongs to secondary field. In this formula, $\kappa_D(\omega)$ is the dynamic permeability and L_{12} is the electrokinetic coupling coefficient

$$\kappa_D(\omega) = -\frac{1}{K^2}\left[\varphi - \frac{2\varphi}{K\sqrt{\frac{8k}{\varphi}}}\frac{J_1\left(K\sqrt{\frac{8k}{\varphi}}\right)}{J_0\left(K\sqrt{\frac{8k}{\varphi}}\right)}\right] \tag{11}$$

$$L_{12} = -\frac{\varepsilon\zeta}{\mu(1+K^2\lambda_D^2)}\left[\begin{array}{c}\frac{2\varphi}{K\sqrt{\frac{8k}{\varphi}}}\frac{J_1\left(K\sqrt{\frac{8k}{\varphi}}\right)}{J_0\left(K\sqrt{\frac{8k}{\varphi}}\right)} \\ -2\varphi\left(\lambda_D\sqrt{\frac{\varphi}{8k}} - \frac{\lambda_D^2\varphi}{8k} + \frac{\lambda_D^2\varphi}{8k}e^{\frac{-1}{\lambda_D}\sqrt{\frac{8k}{\varphi}}}\right)\end{array}\right] \tag{12}$$

Under the influence of pressure gradient, the flow of formation water in rock pore carries ions to move together, and the flow current is as follows

$$j_1 = 2\pi\int_0^{r_0} u(r)\rho_e r\,dr = L_1(w)\frac{\partial P}{\partial z} - L_2(w)\frac{\partial U}{\partial z} \tag{13}$$

In this formula,

$$L_1(W) = -\frac{2FZC_0\varphi}{K^2\mu}\left[\begin{array}{c}\sum_{n=1}^{\infty}\frac{(-ZF\zeta)^n}{(RT)^n n!}\left[\frac{\lambda_D}{n}\sqrt{\frac{\varphi}{8k}} - \frac{\lambda_D^2}{n^2}\frac{\varphi}{8k} + \frac{\lambda_D^2}{n^2}\frac{\varphi}{8k}e^{\frac{-n}{\varphi}\sqrt{\frac{8k}{\varphi}}}\right] \\ -\sum_{n=1}^{\infty}\frac{(ZF\zeta)^n}{(RT)^n n!}\left[\frac{\lambda_D}{n}\sqrt{\frac{\varphi}{8k}} - \frac{\lambda_D^2}{n^2}\frac{\varphi}{8k} + \frac{\lambda_D^2}{n^2}\frac{\varphi}{8k}\right]\end{array}\right]$$

$$+\frac{2FZC_0\varphi}{K^2\mu J_0\left(K\sqrt{\frac{8k}{\varphi}}\right)}\sum_{n=1}^{\infty}\frac{(-ZF\zeta)^n}{(RT)^n n!}\left[\begin{array}{c}\sum_{m=0}^{\infty}\frac{(-1)^m}{(m!)^2}\left(\frac{K}{2}\right)^{2m}\left(\frac{8k}{\varphi}\right)^m \\ \sum_{p=1}^{2m+1}(-1)^{p+1}\left(\frac{\lambda_D}{n}\right)^p\frac{(2m+1)!}{(2m+2-p)!}\left(\frac{8k}{\varphi}\right)^{\frac{p}{2}} \\ -\left(\frac{\lambda_D^2}{n^2}\frac{\varphi}{8k}\right)^{m+1}(2m+1)!+\left(\frac{\lambda_D^2}{n^2}\frac{\varphi}{8k}\right)^{m+1}(2m+1)!e^{\frac{-n}{\lambda_D}\sqrt{\frac{8k}{\varphi}}}\end{array}\right]$$

$$-\frac{2FZC_0\varphi}{K^2\mu J_0\left(K\sqrt{\frac{8k}{\varphi}}\right)}\sum_{n=1}^{\infty}\frac{(ZF\zeta)^n}{(RT)^n n!}\left[\begin{array}{c}\sum_{m=0}^{\infty}\frac{(-1)^m}{(m!)^2}\left(\frac{K}{2}\right)^{2m}\left(\frac{8k}{\varphi}\right)^m \\ \sum_{p=1}^{2m+1}(-1)^{p+1}\left(\frac{\lambda_D}{n}\right)^p\frac{(2m+1)!}{(2m+2-p)!}\left(\frac{8k}{\varphi}\right)^{-\frac{p}{2}} \\ -\left(\frac{\lambda_D^2}{n^2}\frac{\varphi}{8k}\right)^{m+1}(2m+1)!+\left(\frac{\lambda_D^2}{n^2}\frac{\varphi}{8k}\right)^{m+1}(2m+1)!e^{\frac{-n}{\lambda_D}\sqrt{\frac{8k}{\varphi}}}\end{array}\right] \tag{14}$$

$$L_2(w) = -\frac{2FZC_0\varphi\varepsilon\zeta}{\mu(1+K^2\lambda_D^2)J_0\left(K\sqrt{\frac{8k}{\varphi}}\right)}\sum_{n=1}^{\infty}\frac{(-ZF\zeta)^n}{(RT)^n n!}$$

$$\left[\begin{array}{c}\sum_{m=0}^{\infty}\frac{(-1)^m}{(m!)^2}\left(\frac{K}{2}\right)^{2m}\left(\frac{8k}{\varphi}\right)^m\sum_{p=1}^{2m+1}(-1)^{p+1}\left(\frac{\lambda_D}{n}\right)^p\frac{(2m+1)!}{(2m+2-p)!}\left(\frac{8k}{\varphi}\right)^{-\frac{p}{2}} \\ -\left(\frac{\lambda_D^2}{n^2}\frac{\varphi}{8k}\right)^{m+1}(2m+1)!+\left(\frac{\lambda_D^2}{n^2}\frac{\varphi}{8k}\right)^{m+1}(2m+1)!e^{\frac{-n}{\lambda_D}\sqrt{\frac{8k}{\varphi}}}\end{array}\right]$$

$$+\frac{2FZC_0\varphi\varepsilon\zeta}{\mu(1+K^2\lambda_D^2)J_0\left(K\sqrt{\frac{8k}{\varphi}}\right)}\sum_{n=1}^{\infty}\frac{(ZF\zeta)^n}{(RT)^n n!} \tag{15}$$

$$\left\{ \begin{array}{l} \left[\sum_{m=0}^{\infty} \frac{(-1)^m}{(m!)^2} \left(\frac{K}{2}\right)^{2m} \left(\frac{8k}{\varphi}\right)^m \right] \left[\sum_{p=1}^{2m+1} \frac{(-1)^{p+1}\left(\frac{\lambda_D}{n}\right)^p}{n} \frac{(2m+1)!}{(2m+2-p)!}\left(\frac{8k}{\varphi}\right)^{-\frac{p}{2}} \right] \\ \qquad - \left(\frac{\lambda_D^2}{n^2}\frac{\varphi}{8k}\right)^{m+1}(2m+1)! + \left(\frac{\lambda_D^2}{n^2}\frac{\varphi}{8k}\right)^{m+1}(2m+1)! e^{\frac{-n}{\lambda_D}\sqrt{\frac{8k}{\varphi}}} \end{array} \right]$$

$$- \frac{2FZC_0\varphi\varepsilon\zeta}{\mu(1+K^2\lambda_D^2)}\left\{ \begin{array}{l} \sum_{n=1}^{\infty}\frac{(-ZF\zeta)^n}{(RT)^n n!}\left[\frac{\lambda_D}{n+1}\sqrt{\frac{\varphi}{8k}} - \frac{\lambda_D^2}{(n+1)^2}\frac{\varphi}{8k} + \frac{\lambda_D^2}{(n+1)^2}\frac{\varphi}{8k}e^{\frac{-(n+1)}{\lambda_D}\sqrt{\frac{8k}{\varphi}}} \right] \\ -\sum_{n=1}^{\infty}\frac{(ZF\zeta)^n}{(RT)^n n!}\left[\frac{\lambda_D}{n+1}\sqrt{\frac{\varphi}{8k}} - \frac{\lambda_D^2}{(n+1)^2}\frac{\varphi}{8k} + \frac{\lambda_D^2}{(n+1)^2}\frac{\varphi}{8k}e^{\frac{-(n+1)}{\lambda_D}\sqrt{\frac{8k}{\varphi}}} \right] \end{array} \right\} \qquad (15)$$

The conduction current generated by electric field excited by fluid flow is

$$j_2 = 2\pi\int_0^{r_0}\left[F^2Z^2\left(v_+C_+ + v_-C_-\right)E + \varepsilon\frac{dE}{dt} \right]rdr = -L_3(w)\frac{\partial U}{\partial z} \qquad (16)$$

In this formula,

$$L_3(w) = F^2Z^2C_0\varphi(v_+ + v_-)$$

$$+ 2F^2Z^2C_0\varphi\left\{ \begin{array}{l} v_+\sum_{n=1}^{\infty}\frac{(-ZF\zeta)^n}{(RT)^n n!}\left[\frac{\lambda_D}{n}\sqrt{\frac{\varphi}{8k}} - \frac{\lambda_D^2}{n^2}\frac{\varphi}{8k} + \frac{\lambda_D^2}{n^2}\frac{\varphi}{8k}e^{\frac{-n}{\lambda_D}\sqrt{\frac{8k}{\varphi}}} \right] \\ + v_-\sum_{n=1}^{\infty}\frac{(ZF\zeta)^n}{(RT)^n n!}\left[\frac{\lambda_D}{n}\sqrt{\frac{\varphi}{8k}} - \frac{\lambda_D^2}{n^2}\frac{\varphi}{8k} + \frac{\lambda_D^2}{n^2}\frac{\varphi}{8k}e^{\frac{-n}{\lambda_D}\sqrt{\frac{8k}{\varphi}}} \right] \end{array} \right\} - i\pi r_0^2\varepsilon\omega \qquad (17)$$

The current of reservoir rock is

$$j = j_1 + j_2 = L_1(\omega)\frac{\partial P}{\partial z} - \sigma(\omega)\frac{\partial U}{\partial z} \qquad (18)$$

The formula (18) is Ohm's Law of current density in reservoir rocks in frequency domain, and $L_1\frac{\partial P}{\partial z}$ represents flow current. We define L_1 as electrokinetic coupling coefficient and $\sigma(\omega)$ is complex conductivity. The formula (10) and formula (18) give the coupling relationship between current field and seepage field in reservoir rocks in frequency domain.

When the fluid flow process in the reservoir reaches a stable state, the current density generated in the formation is j=0. We call the negative value of the ratio of potential difference ΔU excited by fluid flow to fluid pressure difference ΔP acting on both ends of rock sample as the flow potential coupling coefficient. Therefore, the coupling theory between the current field and the seepage field in the reservoir rock is established. Through the formula (18), it can be obtained,

$$\theta = -\frac{\Delta V}{\Delta P}\bigg|_{j=0} = -\frac{\frac{\partial U}{\partial z}}{\frac{\partial P}{\partial z}}\bigg|_{j=0} = -\frac{L_1(w)}{L_2(w)+L_3(w)} = -\frac{L_1(w)}{\sigma(w)} \qquad (19)$$

2.3 Electroviscous effect and dissipation function of reservoir rocks

2.3.1 Electroviscous effect of reservoir rocks
The electric field produced in the flow potential effect of reservoir rocks acts on the ions in the pore, which makes the ions carry the fluid to flow along the opposite direction of the external pressure gradient through the viscous force, thus impeding the flow of the fluid. This effect is called the electroviscous effect of the fluid. The electroosmotic fluid $L_{12}\frac{\partial U}{\partial z}$ in formula (10) shows this effect, and when the

formula (19) is brought into the formula (10), it can be obtained,

$$v = -\frac{\kappa_D - \mu L_{12}\theta}{\mu}\frac{\partial P}{\partial z} = -\frac{\kappa_D}{\mu_a}\frac{\partial P}{\partial z} \qquad (20)$$

In this formula,

$$\mu_a = \frac{\kappa_D}{\kappa_D - \mu L_{12}\theta}\mu \qquad (21)$$

μ_a is the apparent viscosity of fluid flow, and μ_a/μ is called the apparent viscosity coefficient of fluid, which reflects the reaction of electrokinetic effect of fluid in reservoir rock pore to fluid flow.

2.3.2 Dissipation function of reservoir rock
The loss of energy generated by the electrokinetic effect in unit time and unit section is called the electrokinetic dissipation, and its dissipation function (Medlin *et al.* 1975) expression is

$$D_E = \mathrm{Re}\left\{ j_2^*(w)E_z(w) \right\} = \mathrm{Re}\left\{ l_3^*(w)E_z^2(w) \right\} = \mathrm{Re}\left\{ l_3^*(w)\theta^2(w)\left(\frac{\partial P}{\partial z}\right)^2 \right\} \qquad (22)$$

When the formula (19) are brought into formula (22), it can be obtained

$$D_E = \left\{ \left|\frac{L_1(\omega)}{L_2(\omega)+L_3(\omega)}\right|^2 \left(\begin{array}{l} F^2Z^2C_0\varphi(v_+ + v_-) + 2F^2Z^2C_0\varphi \\ \left(\begin{array}{l} v_+\sum_{n=1}^{\infty}\frac{(-ZF\zeta)^n}{(RT)^n n!}\left[\frac{\lambda_D}{n}\sqrt{\frac{\varphi}{8k}} - \frac{\lambda_D^2}{n^2}\frac{\varphi}{8k} + \frac{\lambda_D^2}{n^2}\frac{\varphi}{8k}e^{\frac{-n}{\lambda_D}\sqrt{\frac{8k}{\varphi}}} \right] \\ + v_-\sum_{n=1}^{\infty}\frac{(ZF\zeta)^n}{(RT)^n n!}\left[\frac{\lambda_D}{n}\sqrt{\frac{\varphi}{8k}} - \frac{\lambda_D^2}{n^2}\frac{\varphi}{8k} + \frac{\lambda_D^2}{n^2}\frac{\varphi}{8k}e^{\frac{-n}{\lambda_D}\sqrt{\frac{8k}{\varphi}}} \right] \end{array} \right) \end{array} \right) \right\}\left(\frac{\partial P}{\partial z}\right)^2 \qquad (23)$$

The formula (23) is the expression of electrokinetic dissipation of reservoir rocks.

The fluid is viscous. When flowing in the channel, the resistance caused by the viscosity of the fluid is called viscous resistance. It is also called internal friction. The viscous resistance causes energy loss that is called viscous resistance dissipation whose size depends on the shear velocity gradient. According to the hydrodynamics, its dissipation function can be expressed by the following formula,

$$D_v = \mu\int_0^{r_0}\left(\frac{\partial u}{\partial r}\right)^*\frac{\partial u}{\partial r}2\pi rdr \qquad (24)$$

When the formula (8) is brought into the formula (24), it can be obtained,

$$D_v = 2\pi\mu|\alpha_1|^2\left\{ \begin{array}{l} \sum_{s=1}^{\infty}\sum_{t=1}^{\infty}\frac{(-1)^{s+t}}{\left[(2s)!(2t)!\right]^2}\frac{16st}{4}\frac{(\beta r_0)^{4(s+t)}}{(s+t)} \\ +\sum_{s=0}^{\infty}\sum_{t=0}^{\infty}\frac{(-1)^{s+t}}{\left[(2s+1)!(2t+1)!\right]^2}\frac{4(2s+1)(2t+1)}{4}\frac{(\beta r_0)^{4(s+t)+4}}{(s+t)+4} \end{array} \right\}\left(\frac{\partial P_z}{\partial z}\right)^2$$

$$+ 2\pi\mu|\alpha_2|^2\left[\frac{\lambda_D}{2}r_0 - \left(\frac{\lambda_D}{2}\right)^2 + \left(\frac{\lambda_D}{2}\right)^2\exp\left(\frac{-2r_0}{\lambda_D}\right)\right]\left(\frac{\partial P_z}{\partial z}\right)^2 \qquad (25)$$

$$+ 4\pi\mu\left[\mathrm{Re}(\alpha_1)\mathrm{Re}(\alpha_2) + \mathrm{Im}(\alpha_1)\mathrm{Im}(\alpha_2)\right]\sum_{n=1}^{\infty}\frac{(-1)^n 4n}{\left[(2n)!\right]^2}\left[\begin{array}{l} \sum_{p=1}^{\infty}\frac{(-1)^{p+1}(4n)!(\lambda_D)^p}{(4n+1-p)!}\beta^{4n}r_0^{4n+1-p} \\ -(4n)!\beta^{4n}\lambda_D^{4n+1}\left[1-\exp\left(\frac{-r_0}{\lambda_D}\right)\right] \end{array} \right]\left(\frac{\partial P_z}{\partial z}\right)^2$$

$$+ 4\pi\mu \left[\text{Re}(\alpha_1)\,\text{Im}(\alpha_2) - \text{Im}(\alpha_1)\,\text{Re}(\alpha_2) \right] \sum_{n=0}^{\infty} \frac{(-1)^{n-1} 2(2n+1)}{\left[(2n+1)!\right]^2} \left\{ \sum_{p=1}^{4n+2} \left(\begin{array}{l} (-1)^{p+1} \dfrac{(4n+2)!\,(\beta)^p\,(\lambda_D)^p\,r_0^{\,4n-3-p}}{(4n+3-p)!} \\ -(\beta)^{4n+2}\,\lambda_D^{\,4n+3}(4n+2)! \left[1 - \exp\left(\dfrac{-r_0}{\lambda_D}\right) \right] \end{array} \right) \right\} \quad (25)$$

In this formula

$$\alpha_1 = -\frac{\varepsilon\xi\theta}{\mu(1+K^2\lambda_D^2)J_0(Kr_0)} - \frac{1}{K^2\mu J_0(Kr_0)},$$

$$\alpha_2 = \frac{\varepsilon\xi\theta}{\mu\lambda_D(1+K^2\lambda_D^2)J_0(Kr_0)}.$$

The formula (25) is the expression of the viscous resistance dissipation of the reservoir rock.

It can be seen from the above formula that there is a complex functional relationship between the electrokinetic dissipation as well as the dissipation of the viscous resistance of the reservoir rock and the frequency as well as the electrochemical parameters of the rock.

3. Calculation examples

According to the above mathematical model, the electrokinetic dissipation caused by elastic wave of reservoir rock is simulated mathematically. Through obtaining a group of porosity φ and permeability k from the original core data of the specific oilfield, the micro-parameter of capillary model of reservoir rock is determined, and the permeability k is determined by using the relationship between reservoir porosity and permeability in reference(Vinogradov *et al.* 2011). In addition, in practical calculation, the porosity φ in the formation should be corrected as φ occupied by the fluid flow channel, the correction formula is $\varphi \Rightarrow 1-(1-\varphi)^{1/3}$, and the cation exchange capacity should be corrected as $Q_v \Rightarrow \varphi \cdot Q_v$ in the calculation of this chapter.

3.1 Distribution of periodic electroosmotic flow velocity

When the fluid flows in the pore, the function of pressure (force) is to change the original state of the fluid. When the fluid accelerates, the function of fluid viscous force (reaction force) and inertia force (reaction force) is to maintain the original state of motion of the fluid. Therefore, the motion state of fluid is the result of the interaction between the action force and the reaction force. The modulus and phase of electrokinetic velocity reflect the magnitude of action force and reaction force respectively. Large modulus value represents the dominant role of pressure, and large phase represents the dominant role of inertia force. According to the above theory, the calculation parameters are selected as shown in Table 1 and the frequency range is $1 \sim 10^6 Hz$. The distribution of periodic electrokinetic velocity along the pore section is calculated by formula (20), as shown in Fig. 4(a). Because the velocity distribution presents different states in the low frequency range and the high frequency range, F = 1000Hz (low frequency range) and 60000Hz (high frequency range) are taken to make velocity distribution diagram. As shown in Fig. 4(b)-4(c), the solid line represents the modulus *v* of the

(a) Overall distribution

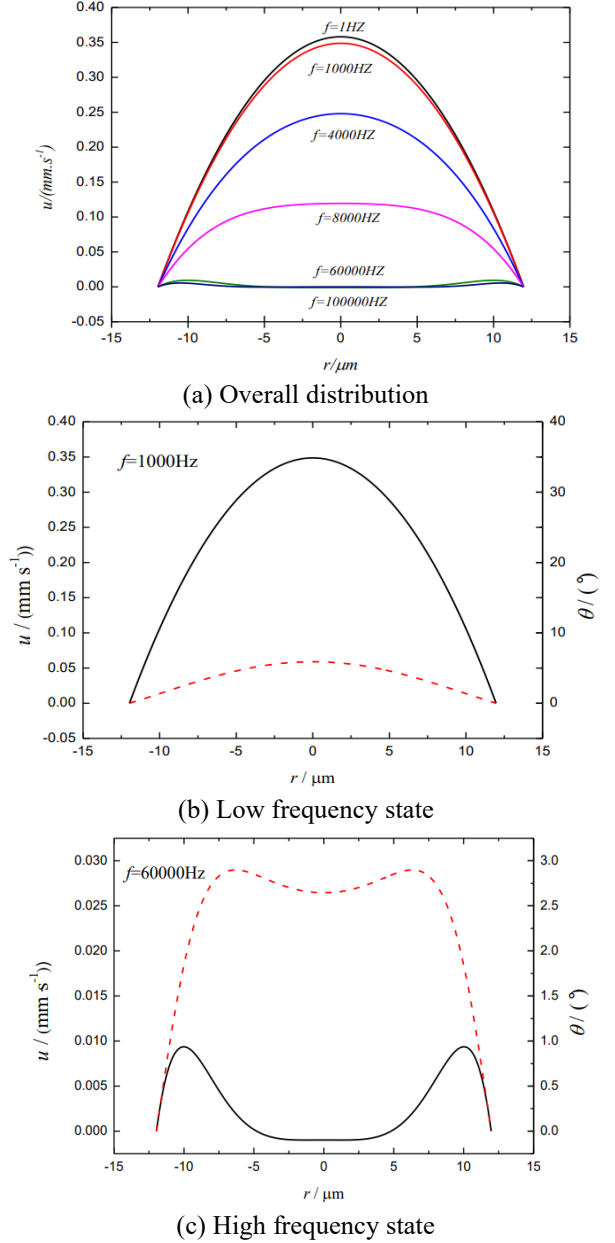(b) Low frequency state

(c) High frequency state

Fig. 4 Distribution of periodic electroosmotic flow velocity along the pore section

electrokinetic velocity and the dotted line represents the phase θ of the electrokinetic velocity. As can be seen from Fig. 4(a)-4(b), the fluid in the pore is mainly affected by pressure at low frequencies. The inertia force is weak and the phase of the fluid is small. Therefore, the velocity of the fluid in the pore center region is much higher than that near the pore wall. The velocity profile of electrokinetic current is approximately parabolic, which is similar to the flow velocity distribution of viscous fluid. With the increase of frequency, the electrokinetic velocity decreases, while the phase, the fluid acceleration, and the lag effect of inertial force on velocity all increase. As shown in Fig. 4(a)-4(c), the velocity in the central region decreases significantly. It can be seen from the literature that the channel wall is mainly affected by the action of electric double layer, and the inertia force can be neglected. Therefore, the fluid

velocity in the pore center region will always lag behind that near the wall, and the electrodynamic velocity profile of pore will be wavy. This is consistent with the experimental conclusion given in reference (Vinogradov *et al.*2011). The electrokinetic flow in the main flow region is almost stagnant, and there is a reflux phenomenon between the electric double layer region and the main flow region. It can also be found from figure (a) that with the increase of frequency, the fluid oscillation in the pore increases, the inertia force of the fluid in the pore increases gradually, and the fluid velocity decreases gradually.

3.2 Electroviscous effects of fluids in reservoir rocks

The flow potential in the porous medium is due to the flow of ions in the pores with the fluid. The apparent viscosity coefficient is the reaction of the reaction flow potential effect on the fluid flow. A certain frequency of pressure is added to both ends of the reservoir rock. According to Darcy's Law, when the frequency is low, the fluid in the pore is subjected to pressure to exhibit a turbulent state, the ions in the pore have sufficient time to move to the ends of the pore to form strong flow potential, and the flow potential has the greatest effect on the fluid. With the increase of frequency, fluid flow oscillation accelerates, most of the ions can't reach both ends of the pore. The hindrance of electrokinetic effect on fluid weakens.

According to the above theory, the corresponding parameters are selected from Table 1, the frequency is changed, and the dispersion characteristics of the apparent viscosity coefficient of the porous medium can be obtained as shown in Fig. 5. The modulus in the figure is the porosity, concentration, and cation exchange capacity. The solid line indicates the modulus value of the apparent viscosity coefficient, and the dotted line indicates the phase of the apparent viscosity coefficient. It can be seen from Fig 5 that the modulus of apparent viscosity coefficient exhibits a maximum value when the frequency is weak. As the frequency increases, the phase gradually increases, and the modulus of apparent viscosity coefficient gradually decreases toward 1, and the intersection of the two represents the critical frequency. The formula (21) is used to calculate the relationship between apparent viscosity coefficient and porosity, solution concentration and cation exchange capacity. According to Fig. 5, the larger the porosity is, the smaller the apparent viscosity coefficient is. This is because when the thickness of the electric double layer is fixed, the larger the porosity is, the smaller the proportion of the electric double layer affecting the fluid flow space is, and the weaker the hindrance to the fluid flow is. The effect of solution concentration on apparent viscosity coefficient is shown in Fig. 5(b). The bigger the solution concentration is, the thinner the thickness of the electric double layer is. The weaker the electrokinetic coupling ability of the fluid is, the smaller the hindrance of the electric field on the flow of the fluid is, and the smaller the apparent viscosity coefficient is. The effect of solution concentration on apparent viscosity coefficient is shown in Fig. 5(c). The larger the cation exchange capacity is, the more ions are adsorbed on the solid-liquid interface. The

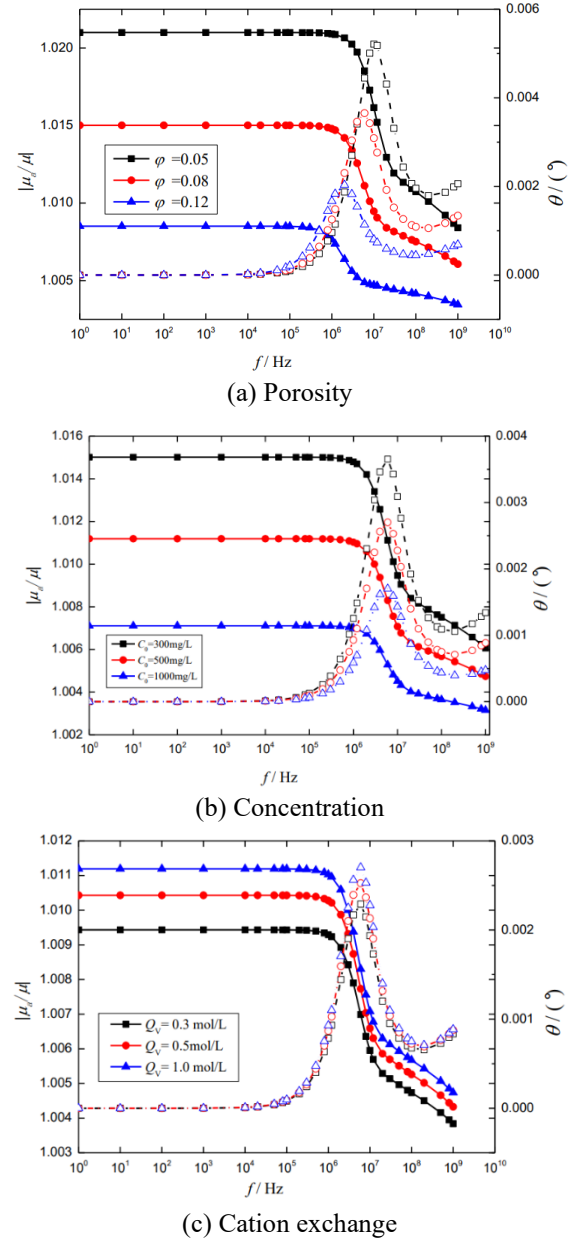(a) Porosity

(b) Concentration

(c) Cation exchange

Fig. 5 Impact of the reservoir parameters on frequency dispersion characteristics of the apparent viscosity coefficient

larger the Zeta potential is, the more obvious the hindrance of the electric field on the flow of the fluid is, and the larger the apparent viscosity coefficient is.

3.3 Relationships between electrokinetic effect, viscous resistance and ratio

According to formula (23) and (25), Fig 6 shows the dispersion characteristics of viscous resistance dissipation and electrokinetic dissipation, and compares the two. It can be seen from Fig. 6(a) that in the low frequency state, the fluid velocity in the pore decreases with increasing frequency, and the distribution along the diameter becomes more and more gradual, and the viscous resistance dissipation function decreases. In the high-frequency state,
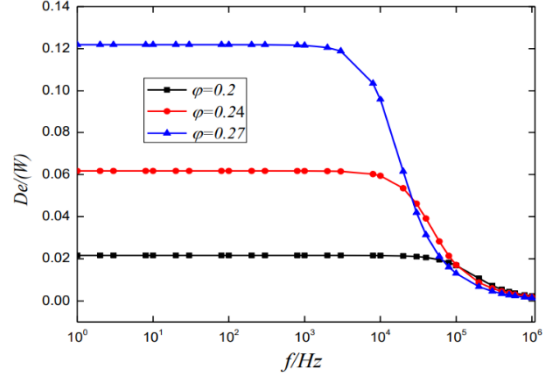
(a) Viscous resistance dissipation function

(a) Viscous resistance dissipation function
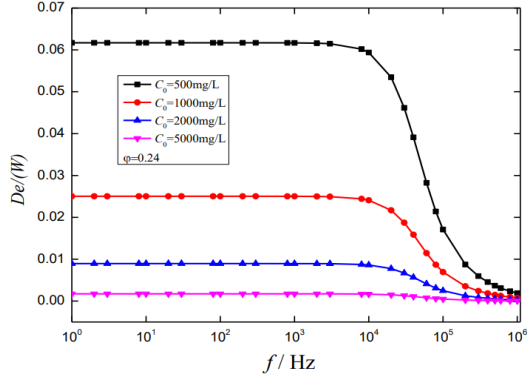
(b) Electrokinetic dissipation function
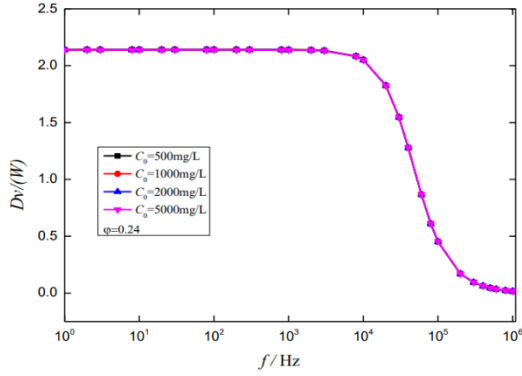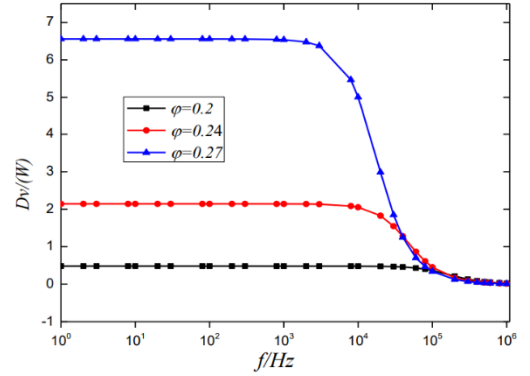

(b) Electrokinetic dissipation function
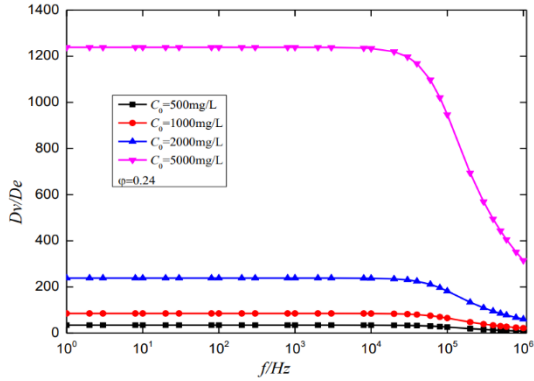
(c) Ratio

(c) Ratio

Fig. 6 Relationship between viscous resistance dissipation, electrokinetic dissipation, ratio and solution concentration

Fig. 7 Relationship between viscous resistance dissipation, electrokinetic dissipation, ratio and porosity
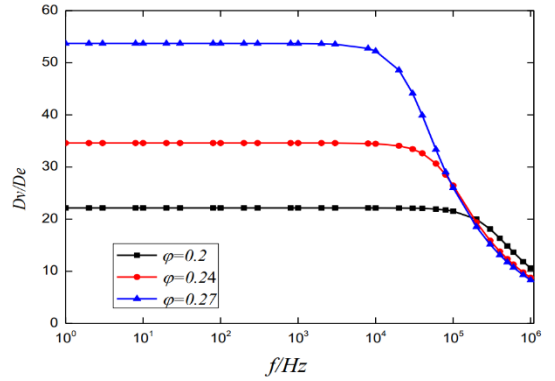
the frequency is further increased, the change rate of fluid velocity along diameter in pore tends to zero, and the viscous resistance dissipation function approaches zero, which is consistent with the results obtained in Fig. 6(a). The electrolyte solution with charge flows under the influence of pressure gradient, and the resulting flow potential is an obstacle to fluid flow. With the increase of frequency, the flow potential decreases, and the dissipation function of electrokinetic effect decreases, and finally approaches zero. By comparing the two, it can be seen from Fig. 6(c)that the electrokinetic dissipation plays a certain role in fluid flow, which explains that the flow rate of micro-scale fluid in experimental data is much smaller than that calculated by traditional theory, but the dissipation of viscous resistance is two orders of magnitude higher than

that of electrokinetic effect. From Fig. 6, it can also be seen that the electrokinetic effect plays a role in the fluid flow in the pore at low frequency, but when the frequency is very high, the dissipation caused by the electrokinetic effect can be neglected. Fig. 6 also shows the relationship curve between viscous resistance dissipation function and electrokinetic dissipation function as well as concentration. The greater the solution concentration is, the thinner the electric double layer thickness is. The fluid viscosity in the pore becomes weaker, the fluid velocity decreases, and the dissipation function of viscous resistance decreases. At the same time, the electrokinetic coupling ability of the fluid decreases with the decrease of the thickness of the electric double layer, and the electrokinetic dissipation function decreases. It can also be seen from Fig. 6(b) that the concentration of electrolyte solution has no effect on the

viscous resistance.

3.4 Relationships between electrokinetic effect, viscous resistance and porosity

Fig. 7 shows the relationship between viscous resistance dissipation, electrokinetic dissipation and porosity at different porosity. It can be seen from Fig 7, with the increase of porosity, the flow rate of fluid in the pore increases, the flow capacity increases, and the viscous resistance of fluid increases. At the same time, ions in the pore increase, the electrokinetic effect caused by the electric double layer effect is enhanced, and the electrokinetic dissipation is enhanced. The Fig. 7(c) shows the ratio of viscous resistance dissipation to electrokinetic dissipation and the porosity are given in the figure. From the figure, it can be seen that the ratio increases with the increase of porosity, that is, the rate of increase in dissipation caused by the electrokinetic effect is faster than that of viscous resistance dissipation.

4 Conclusions

At present, the research on the electrokinetic effects dissipation is based on the theory established by Repeat, Yang, etc. These theories do not establish a complete theoretical system of frequency domain electrokinetic dissipation. The theoretical expression contains some hypothetical constants whose physical meaning is not very clear or cannot be measured experimentally. It is difficult to quantitatively explain the electrokinetic dissipation of reservoir rocks. In this paper, Ohm's Law of current density in frequency domain is derived through expanding double layer potential distribution with series and Bessel function method, and then derive the analytical formulas of the electrokinetic effect dissipation function. The analytical formula of viscous resistance dissipation is obtained by hydrodynamics, and the quantitative mathematical description of the electrokinetic dissipation of reservoir rock is realized. The dispersion characteristics of the electrokinetic dissipation of reservoir rocks are studied from the microscopic mechanism. The correctness and reliability of the theory are proved by calculation examples, and the following conclusions are obtained:

(1) At a certain frequency, the electrokinetic effect caused by the elastic wave has a hindrance to the fluid flow, and the energy dissipation caused by the electrokinetic effect is far less than the energy dissipation caused by the viscous resistance. When the concentration of the electrolyte exceeds 0.1mol/L, the electrokinetic dissipation can be neglected; and for the electrolyte solution ($<10^{-2}$M) with low concentration, the electrokinetic dissipation phenomenon becomes very significant. The dissipation of electrokinetic effect decreases with the increase of electrolyte concentration, and increases with the increase of porosity. The concentration of electrolyte solution has no effect on the dissipation of viscous force. The greater the porosity is, the more significant the viscous force dissipation is.

(2) Under the action of the periodic pressure field, the fluid in the pores of the reservoir rock is subjected to pressure, the viscous force and the inertial force. When the frequency is low, the inertial force of the fluid is small, and the fluid in the pores becomes a steady flow state, and the fluid flow profile in the pore is approximate parabola. With the increase of frequency, the fluid flow oscillation accelerates. The inertia force and viscous force of fluid play a dominant role in the fluid flow, and the fluid velocity decreases. At the channel wall, because of the friction force, the velocity of the channel wall is always greater than that of the middle of the pore, so the fluid flow becomes wavy.

(3) The apparent viscosity coefficient reflects the reaction of the flow potential effect of the fluid in the pores of the reservoir rock to the fluid flow. The results show that, at low frequencies, the apparent viscosity coefficient is >1 and is basically unchanged. When the frequency increases to a certain value, the apparent viscosity coefficient gradually approaches 1 as the frequency increases further. The decrease in porosity, the increase in formation water concentration, and the increase in cation exchange capacity all increase the apparent viscosity coefficient.

Because the interpretation of the mechanism of electrokinetic dissipation involves the fluid mechanism of porous media in reservoirs, different fluid models of porous media can be used to obtain different simulation results of electrokinetic dissipation. The physical mechanism model of Biot two-phase medium is chosen in this paper, which can't explain all experimental phenomena and physical causes. Moreover, the complexity of micro-pore structure and fluid flow mechanism of reservoir rocks and the conclusion need further experimental verification.

References

Allègre, V., Jouniaux, L., Lehmann, F. and Sailhac, P. (2010), "Streaming potential dependence on water-content in Fontainebleau sand", *Geophys. J. Int.*, **182**(3), 1248-1266. https://doi.org/10.1111/j.1365-246X.2010.04716.x.

Carcione, J.M. and Tinivella, U. (2000), "Bottom-simulating reflectors: Seismic velocities and AVO effects", *Geophysics*, **66**(3), 984. https://doi.org/10.1190/1.1444725.

Ding, Z., Jian, Y. and Tan, W. (2019), "Electrokinetic energy conversion of two-layer fluids through nanofluidic channels", *Fluid Mech.*, **863**, 1062-1090. https://doi.org/10.1017/jfm.2019.6.

Garambois, S., Sénéchal, P. and Perroud, H. (2012), "On the use of combined geophysical methods to assess water content and water conductivity of near-surface formations", *J. Hydrol.*, **259**(1), 32-48. https://doi.org/10.1016/S0022-1694(01)00588-1.

Ghommem, M., Qiu, X.D., Aidagulov, G. and Abbad, M. (2017), "Streaming potential measurements for downhole monitoring of reservoir fluid flows: A laboratory study", *J. Petrol. Sci. Eng.*, **161**, 38-49. https://doi.org/10.1016/j.petrol.2017.11.039.

Guan, W., Shi, P. and Hu, H. (2018), "Contributions of poroelastic-wave potentials to seismoelectromagnetic wavefields and validity of the quasi-static calculation: A view from a borehole model", *Geophys. J. Int.*, **212**(1), 458-475. https://doi.org/10.1093/gji/ggx417.

Holzhauer, J., Brito, D., Bordes, C., Brun, Y. and Guatarbes, B. (2017), "Experimental quantification of the seismoelectric transfer function and its dependence on conductivity and saturation in loose sand", *Geophys. Prospect.*, **65**(4), 1097-1120.

https://doi.org/10.1111/1365-2478.12448.

Hu, H.S., Wang, K.X. and Wang, J. (2000), "Simulation of acoustically induced electromagnetic field in a borehole embedded in a porous formation", Borehole Acoustics Annual Report, Earth Resources Laboratory, Massachusetts Institute of Technology, Cambridge, Massachusetts, U.S.A.

Ji, Y. and Li, X. (2018), "Analysis on Geo-stress and casing damage based on fluid-solid coupling for Q9G3 block in Jibei oil field", *Geomech. Eng.*, **15**(1), 677-686. https://doi.org/10.12989/gae.2018.15.1.677.

Jouniaux, L. and Zyserman, F. (2016), "A review on electrokinetically induced seismo-electrics, electro-seismics, and seismo-magnetics for earth sciences", *Solid Earth*, **7**(1), 249-284. https://doi.org/10.5194/se-7-249-2016.

Liu, N., Huang, Q.B., Fan, W., Ma, Y.J. and Peng, J.B. (2018), "Seismic responses of a metro tunnel in a ground fissure site", *Geomech. Eng.*, **15**(2), 775-781. https://doi.org/10.12989/gae.2018.15.2.775.

Peng, R., Di, B., Wei, J., Ding, P., Zhao, J., Pan, X. and Liu, Z. (2017), "Experimental study of the seismoelectric interface response in wedge and cavity models", *Geophys. J. Int.*, **210**(3), 1703-1720. https://doi.org/10.1093/gji/ggx253.

Pride, S.R. (1994), "Governing equations for the coupled electromagnetics and acoustics of porous media", *Phys. Rev. B*, **50**(21), 15678-15696. https://doi.org/10.1103/PhysRevB.50.15678.

Revil, A. (2016), "Transport of water and ions in partially water-saturate d porous media. Part 1. Constitutive equations", *Adv. Water Resour.*, **103**, 119-138. https://doi.org/10.1016/j.advwatres.2016.02.006.

Revil, A., Barnier, G., Karaoulis, M., Sava, P., Jardani, A. and Kulessa, B. (2013), "Seismoelectric coupling in unsaturated porous media: theory, petrophysics, and saturation front localization using an electroacoustic approach", *Geophys. J. Int.*, **196**(2), 867-884. https://doi.org/10.1093/gji/ggt440.

Revil, A., Kessouri, P. and Torres-Verdín, C. (2014), "Electrical conductivity, induced polarization, and permeability of the Fontainebleau sandstone". *Geophysics*, **79**(5), D301-D318. https://doi.org/10.1190/geo2014-0036.1.

Shi, P., Guan, W. and Hu, H.S. (2018), "Dependence of dynamic electrokinetic-coupling-coefficient on the electric double layer thickness of fluid-filled porous formations", *Ann. Geophys.*, **61**(3), 340. https://doi.org/10.4401/ag-7522.

Thompson, A.H., Hornbostel, S., Burns, J., Murray, T., Raschke, R., Wride, J., McCammon, P., Summer, J., Haake, G., Bixby, M., Ross, W., White, B.S., Zhou, M.Y. and Peczak, P. (2007), "Field tests of electroseismic hydrocarbon detection", *Geophysics*, **72**(1), N1-N9. https://doi.org/10.1190/1.2399458.

Vinogradov, J. and Jackson, M.D. (2011), "Multiphase streaming potential in sandstones saturated with gas/brine and oil/brine during drainage and imbibition", *Geophys. Res. Lett.*, **38**(1), L01301. https://doi.org/10.1029/2010GL045726.

Walker, E., Glover, P.W.J., Tardif, E. and Ruel, J. (2011), *DC Elcectrokinetic Coupling Coefficient of Porous Samples in the Laboratory: Experimentation and Modeling*, Energy Environment Economy.

Wang, J., Hu, H., Guan, W., Zheng, W., Yang, Y. and Li, H.(2017), "Electrokinetic measurements of formation velocities with wireline seismoelectric logging and seismoelectric logging while drilling", *Chin. J. Geophys.*, **60**(2), 862-872. https://doi.org/10.6038/cjg20170236. (in Chinese).

Xie, Y., Sherwood, J.D., Shui, L.L., Van Den Berg, A. and Eijkel, J.C.T., (2011), "Strong enhancement of streaming current power by application of two phase flow", *Lab on a Chip*, **11**(23), 4006-4011. https://doi.org/10.1039/c1lc20423h.

Zhang, R., Wang, S., Yeh, M.H., Pan, C., Lin, L., Yu, R., Zang, Y., Zheng, L., Jiao, Z. and Wang, Z.L. (2015), "A streaming potential/current-based microfluidic direct current generator for self-powered nanosystems", *Adv. Mater.*, **27**(41), 6482-6487. https://doi.org/10.1002/adma.201502477.

Zhao, G., Jian, Y. and Li, F. (2016), "Heat transfer of nanofluids in microtubes under the effects of streaming potential", *Appl. Therm. Eng.*, **100**, 1299-1307. https://doi.org/10.1016/j.applthermaleng.2016.02.101.

Zyserman, F.I., Gauzellino, P.M., Santos, J.E. (2012), "Numerical evidence of gas hydrate detection by means of electroseismics", *J. Appl. Geophys.*, **86**, 98-108. https://doi.org/10.1016/j.jappgeo.2012.08.005

Zyserman, F.I., Jouniaux, L., Warden, S. and Garambois, S. (2015), "Borehole seismoelectric logging using a shear-wave source: possible application to CO2 disposal?", *Int. J. Greenhouse Gas Control*, **33**, 89-102. https://doi.org/10.1016/j.ijggc.2014.12.009.

Zyserman, F.I., Monachesi, L.B. and Jouniaux, L. (2016), "Dependence of shear wave seismoelectrics on soil textures: A numerical study in the vadose zone", *Geophys. J. Int.*, **208**(2), 918-935. https://doi.org/10.1093/gji/ggw431.

CC